Supporting Information

Akimoto et al. 10.1073/pnas.1312644110

SI Text

SI Materials and Methods

Protein Expression and Purification. Bovine RIα (91-244) was subcloned into a pTriEX vector as a rare codon optimized fusion construct with His_6-small ubiquitin-related modifier (SUMO) connected to the N terminus of RIα by a TEV cleavable linker. RIα (91-244) was then expressed in the *Escherichia coli* strain BL-21(DE3). Cells were grown in M9 minimal media and induced with 0.5 mM isopropyl β-D-1-thiogalactopyranoside at an optical density of 0.6–0.9 (λ = 600 nm), and further incubated at 18–20° for 16 h. After harvesting, the cells were resuspended in the lysis buffer (50 mM Mops, pH 7 with 100 mM NaCl) and lysed by French press. The cell lysate was centrifuged and the supernatant was further purified by nickel-NTA (nitrilotriacetic acid) affinity chromatography with wash buffer (50 mM Mops, pH 7 with 0.5 M NaCl and 20 mM imidazole) and elution buffer (50 mM Mops, pH 7 with 0.5 M NaCl and 250 mM imidazole). The His_6-SUMO was cleaved by His_6-tagged tobacco etch virus (TEV) protease before a second Ni^{2+} column purification to remove both the cleaved His_6-SUMO and TEV. The cleaved protein was purified by gel filtration on a Superdex 75 column. Uniformly ^{13}C and ^{15}N labeled RIα (96-244) subcloned into the pRSET vector was expressed and purified according to the previously described protocols for RIα (119-244). To prepare the *apo* sample, the purified protein was unfolded with 8 M urea and passed through a PD10 column. The protein was then refolded by dialysis against a 20-mM Mops buffer (pH 7 containing 100 mM KCl, 5 mM β-ME, and 0.5 mM EDTA) with two buffer exchanges. After refolding, the protein was further purified through size exclusion chromatography. All mutants were prepared by site-directed mutagenesis.

H/H Exchange. The H/H exchange rates between water and the backbone amide protons were measured using the clean chemical exchange-phase modulated (CLEANEX-PM)-FHSQC (fast HSQC) experiment (1) for Rp-cAMPS- and cAMP-bound ^{15}N-labeled RIα (91-244). For this purpose, the protein was concentrated to 10 μM in 50 mM Mops (pH 7), 100 mM NaCl, 10 mM $MgCl_2$, 5 mM DTT, 0.02% sodium azide, and 5% ^2H_2O. For the cAMP- and Rp-cAMPS-bound states, 1 mM cAMP and 1 mM Rp-cAMPS were added to the protein samples, respectively. The ^1H and ^{15}N carrier frequencies were set at the water resonance and in the middle of the amide region, respectively. A total of 88 scans were accumulated with an interscan delay of 2 s and an rf strength of 6.9 kHz for the CLEANEX-PM mixing block, which minimizes offset effects. The mixing time was 80 ms.

Urea Unfolding. *apo* RIα (91-244) and *apo* RIα (119-244) were incubated for 3 h at room temperature with increasing concentrations of urea (0–8 M). For the cAMP- and Rp-cAMPS-bound samples, 100-fold excess cAMP and Rp-cAMPS in the assay buffer (50 mM Mops, pH 7 containing 100 mM NaCl, 10 mM $MgCl_2$) were used. The final protein concentration was 5 μM. All fluorescence measurements were performed with a TECAN infinite M200. The samples were excited at 293 nm and the resulting emission spectra were followed from 335 to 365 nm. The fluorescence intensity ratio (353 nm/340 nm) was used to follow the shift in wavelength caused by the unfolding of the cAMP-binding domain A (CBD-A) (2). Unfolding curves (Fig. S3) were calculated using the following equation: $X_U = (R_{obs}-R_N)/(R_U-R_N)$, where X_U is the fraction of unfolded protein and R_{obs} is the observed ratio of intensity at various urea concentrations. R_N and R_U are R_{obs} of the fully folded and unfolded states, respectively. A two-state model was used to calculate the free energy of unfolding ΔG according to $\Delta G_{unfolding} = -RT \ln(X_U/X_N)$ with $X_N + X_U = 1$, where X_N is the fraction of native protein. ΔG^{H20} and m were calculated using the equation $\Delta G = \Delta G^{H_2O} + m[Urea]$, where ΔG^{H_2O} is the free energy of unfolding in the absence of denaturant.

NMR of the Holoenzyme RIα (91-244):C Complex. $^2H,^{15}N$-labeled RIα (91-244) was prepared using deuterated M9 media. The C-subunit of protein kinase A (PKA) was expressed and purified from the *E. coli* strain BL-21(DE3) according to established protocols (3). Holoenzyme was formed overnight by mixing PKA C and *apo* $^2H,^{15}N$-labeled RIα (91-244) at a 1.2:1 ratio and purified by gel filtration to separate the RIα (91-244):C complex from the free RIα (91-244). The holoenzyme sample was then concentrated to 0.2 mM in 50 mM Mops (pH 7), 100 mM NaCl, 10 mM $MgCl_2$, 5 mM DTT, 1 mM AMP-PNP, 0.02% sodium azide, and 5% ^2H_2O. Transverse-relaxation optimized spectroscopy (TROSY) 2D experiments with 80 (t_1) and 1024 (t_2) complex points and spectral widths of 31.82 and 15.94 ppm for the ^{15}N and ^1H dimensions, respectively, were recorded with 12 scans and a recycle delay of 1.70 s.

NMR of RIα (91-379). $^2H,^{15}N$-labeled RIα (91-379) was prepared using deuterated M9 media. The *apo* sample was prepared according to the previously described protocols for the RIα (91-244). *apo* $^2H,^{15}N$-labeled RIα (91-379) was concentrated to 0.2 mM in 50 mM Mops (pH 7), 100 mM NaCl, 10 mM $MgCl_2$, 5 mM DTT, 0.02 mM ^{15}N-acetylglycine, 0.02% sodium azide, and 5% ^2H_2O. For the cAMP-bound states, 1 mM cAMP was added to the protein samples. Holoenzyme was formed according to the protocol for the holoenzyme sample of RIα (91-244) as described above. The holoenzyme sample was then concentrated to 0.2 mM in 50 mM Mops (pH 7), 100 mM NaCl, 10 mM $MgCl_2$, 5 mM DTT, 1 mM 5′-Adenylyl imidodiphosphate (AMP-PNP), 0.02% sodium azide, and 5% ^2H_2O. TROSY 2D experiments with 80 (t_1) and 1024 (t_2) complex points and spectral widths of 31.82 and 15.94 ppm for the ^{15}N and ^1H dimensions, respectively, were recorded with 80 scans and a recycle delay of 1.70 s.

Spin Labeling and Paramagnetic Relaxation Enhancement Analysis. Ala109Cys PKA RIα (91-244) was prepared according to the protocol used for wt RIα (91-244), but during the purification of the mutant, DTT or β-mercaptoethanol was added to the buffer. The spin label 1-oxyl-2,2,5,5-tetra-methyl-pyrroline-3-methyl-16 methanethiosulfonate (MTSL) was covalently attached to the free cysteine residue in the mutant Ala109Cys PKA RIα (91-244). The reducing reagent was exchanged using a PD10 column before the addition of MTSL. The reduced mutated PKA RIα (91-244) was incubated with a threefold molar excess of MTSL for 3 h at room temperature. After the excess MTSL was removed using a PD10 column, 2 mM Rp-cAMPS was added to 10 μM *apo* mutated PKA RIα (91-244). To prepare the cAMP-bound sample, 2 mM cAMP was added to 10 μM *apo* mutated PKA RIα (91-244). The PRE ^1H transverse relaxation rates were obtained from two time-points measurements (4) for both the cAMP- and the Rp-cAMPS-bound sample. The detection block for the PRE experiments was a sensitivity-enhanced $^1H^{15}N$ hetero-nuclear single quantum coherence (HSQC) with 256 (t_1) and 1024 (t_2) complex points and spectral widths of 31.82 and 14.06 ppm for the ^{15}N and ^1H dimensions, respectively. Ninety-six scans were recorded with a recycle delay of 1.50 s. The variation in the PRE relaxation delay (ΔT) was optimized to 5.9 ms. After recording the data for the paramagnetic

state, 5 mM DTT was added to obtain the diamagnetic control for both the cAMP- and the Rp-cAMPS-bound samples. The diamagnetic sample was incubated at room temperature for 1 h, after which we repeated the same experiments carried out for the paramagnetic sample. The H^N Γ_2-rates were then quantified as previously described (4).

Measurement of PKA Holoenzyme Activation by cAMP. The activity of recombinant purified C subunit was determined by a luminescent kinase assay (Kinase-Glo, Promega) that quantifies decrements in ATP due to kinase activation. The PKA holoenzyme was exposed (5 min, 20 °C) to cAMP (0.1–10 μM), after which 5 μM Kemptide and 4 μM ATP were added and allowed to react for 60 min in 50 μL assay buffer (Tris·HCl 40 mM pH 7.5, BSA 0.1 mg/mL, and $MgCl_2$ 20 mM). Reactions were stopped by adding 50 μL of the Ultra-Glo Luciferase reagent (Promega), which was incubated for an additional 10 min at room temperature. Luminescence was measured with a TECAN infinite M200 microplate luminometer.

Inhibition of PKA Activity by RIα (91-244). The catalytic subunit (4 nM) was incubated with different concentrations of RIα (91-244) for 10 min at room temperature. A mixture of Kemptide 50 μM and 10 μM ATP was added to 50 μL assay buffer (Tris·HCl 40 mM pH 7.5, BSA 0.1 mg/mL, and $MgCl_2$ 20 mM) to start the phosphorylation reaction. A mixture of the catalytic subunit (4 nM) and 10 μM ATP without Kemptide was prepared as a positive control sample in 50 μL assay buffer. After 60 min, the reaction was stopped by adding 50 μL of the Ultra-Glo Luciferase solution to the reaction solution and incubating for 10 min. Luminescence was measured with a TECAN ULTRA Evolution spectrophotometer. Normalized relative luminescence units (RLU) were calculated by subtracting the luminescence of the free catalytic subunit sample from that of all samples and dividing by the luminescence of the positive control, which was also corrected by subtracting the luminescence of the free catalytic subunit.

Singular Value Decomposition Analysis of the Chemical Shift Matrix. Singular value decomposition (SVD) analysis indicates that the first two principal components (PCs) alone account for more than 90% of the total variance (Table S2) and Fig. S4*C* shows the PC1 vs. PC2 map of the residue-specific scores (black circles) and of the perturbation-specific loadings (red diamonds). The loadings with the largest component along PC1 correspond to differences between active and inactive forms of R_A, which are all ligand-bound (e.g., cAMP–Rp-cAMPS, Fig. S4*C*), indicating that PC1 reports primarily on allosteric activation as opposed to binding. Unlike PC1, the second PC reports mainly on binding rather than activation, because the loading with the largest component along PC2 corresponds to differences between the *apo* and the Rp-cAMPS-bound states (Fig. S4*C*), which are both inactive. The SVD scores for the residues in the largest agglomerative clustering (AC) cluster (Fig. 3*B*) are distributed mostly along PC1 (Fig. S4*C*, gray filled circles), confirming that the AC network, which includes the linker, is functionally linked to the cAMP-dependent allosteric activation of PKA.

Thermodynamic Modeling of the cAMP-Dependent Activation of PKA. The first step in the thermodynamic model of the cAMP-dependent activation of PKA is to consider that in the absence of cAMP (*apo* form) the inhibiting R-subunit construct RIα (91-244) exists as an equilibrium between the inhibiting (inactive) conformation, denoted as H, and the active conformation, denoted as B. If L is defined as the equilibrium constant for the H vs. B equilibrium in the *apo* form

$$L = [H]_{apo}/[B]_{apo}, \quad \textbf{[S1]}$$

then the $[H]_{total}/[B]_{total}$ ratio in the presence of cAMP defines an apparent equilibrium constant $L_{app.}$ computed as

$$L_{app.} = L\left(1 + K_{a,R(H):cAMP}[\mathrm{cAMP}]\right)/\left(1 + K_{a,R(B):cAMP}[\mathrm{cAMP}]\right), \quad \textbf{[S2]}$$

where [cAMP] is the concentration of free cAMP, whereas $K_{a,R(H):cAMP}$ and $K_{a,R(B):cAMP}$ are the association constants between cAMP and RIα (91-244) in the H and B conformations, respectively. The apparent equilibrium constant L_{app} is then used to compute the overall molar fractions of the H and B conformations, i.e., x_H and x_B, at any given concentration of cAMP, as

$$x_H = L_{app.}/\left(1 + L_{app.}\right), \quad \textbf{[S3]}$$

$$x_B = 1 - x_H. \quad \textbf{[S4]}$$

The molar fractions of the H and B conformations are in turn used for calculating the conformation-average association constant between RIα (91-244) and the catalytic subunit of PKA (i.e., C):

$$K_{a,R:C} = x_H K_{a,R(H):C} + x_B K_{a,R(B):C}, \quad \textbf{[S5]}$$

where $K_{a,R(H):C}$ and $K_{a,R(B):C}$ are the association constants between C and RIα (91-244) in the H and B conformations, respectively. Note that Eqs. **S1–S5** can also be derived by differentiating with respect to [C] the binding polynomial based on the thermodynamic linkage model of Fig. 4*A*: $Q = L(1 + K_{a,R(H):C}[C])(1 + K_{a,R(H):cAMP}[\mathrm{cAMP}]) + (1 + K_{a,R(B):C}[C])(1 + K_{a,R(B):cAMP}[\mathrm{cAMP}])$. In principle, $K_{a,R:C}$ computed according to Eq. **S5** should be downscaled to account for the competing effect of the Kemptide substrate binding to C. However, the downscaling factor caused by the competitive binding of Kemptide is $(1 + [\mathrm{Kemptide}]/K_{d,Kemptide:C})$, which is negligible considering that $K_{d,Kemptide:C}$ is estimated at ∼300 μM (5) and that under our experimental conditions [Kemptide] ≤ 5 μM. We therefore relied on Eq. **S5** for the calculation of the $K_{a,R:C}$ association constant, which was then used to compute the average fraction of inhibited C, i.e., bound to RIα (91-244), or $\langle\nu\rangle$ at any given concentration of cAMP as

$$\langle\nu\rangle = \left\{\beta - \sqrt{\left(\beta^2 - 4[R]_{tot.}[C]_{tot.}\right)}\right\}\Big/\left(2[C]_{tot.}\right), \quad \textbf{[S6]}$$

where $\beta = [R]_{tot.} + [C]_{tot.} + (1/K_{a,R:C})$ and $[R]_{tot.}$ and $[C]_{tot.}$ are the total concentrations of RIα (91-244) and C, respectively.

Eqs. **S1–S6** were used to compute $\langle\nu\rangle$ at different concentrations of free cAMP. However, the concentrations of free cAMP are often not experimentally available and only the total concentrations of cAMP are measured. To circumvent this problem the concentration of free cAMP can be computed from the total concentration of cAMP through the following approximations. First, we consider that under the experimental conditions used for the measurement of the activation of PKA,

$$[R]_{tot.} > [C]_{tot.} >> K_{d,R:C}. \quad \textbf{[S7]}$$

The inequalities in [S7] imply that in the absence of cAMP essentially all C is bound to R and excess free R is present in the amount of

$$[R]_{free} \approx [R]_{tot.} - [R{:}C] \quad \textbf{[S8]}$$

with $[R{:}C] \approx [C]_{tot}$ at the beginning of the cAMP titration. (The concentration of [R:C] for subsequent points in the cAMP titration is estimated based on the computation of $\langle\nu\rangle$ for the preceding total cAMP concentration considered.) The excess free R acts as a high-affinity sink for cAMP that depletes the cAMP pool available for targeting the R:C complex, which exhibits a lower affinity for cAMP. However, the high-affinity sink effect arising from the

excess free R can be easily modeled once $[R]_{free}$ and $K_{a,R:cAMP}$ are known:

$$[cAMP]_{free} = [cAMP]_{tot} - 0.5\left\{\gamma - \sqrt{\left(\gamma^2 - 4[R]_{free}[cAMP]_{tot.}\right)}\right\}, \quad \textbf{[S9]}$$

where $\gamma = [R]_{free} + [cAMP]_{tot.} + (1/K_{a,R:cAMP})$ and

$$K_{a,R:cAMP} = x_{H,apo}K_{a,R(H):cAMP} + x_{B,apo}K_{a,R(B):cAMP}. \quad \textbf{[S10]}$$

Eqs. **S9** and **S10** allow the computation of $[cAMP]_{free}$ starting from $[cAMP]_{tot}$.

In conclusion, using Eqs. **S1–S10** the fraction of C bound to R (i.e., $<\nu>$) is computed for each $[cAMP]_{tot}$ value considered. $[cAMP]_{tot}$ was varied between a minimum of 1 nM and a maximum of 1 mM and the resulting calculated $<\nu>$ vs. $[cAMP]_{tot}$ function was used to model the experimental RLU profile, assuming that the $<\nu>$ computed at the minimum and maximum $[cAMP]_{tot}$ correspond to the maximum and minimum measured RLU values, respectively. Overall, the computation of $<\nu>$ vs. $[cAMP]_{tot}$ based on Eqs. **S1–S10** relies on five key thermodynamic constants: $K_{a,R(H):cAMP}$ and $K_{a,R(B):cAMP}$, which together define the affinity and the H vs. B selectivity of cAMP for RIα (91-244), $K_{a,R(H):C}$ and $K_{a,R(B):C}$, which together define the affinity and the H vs. B selectivity of C for RIα (91-244), and L, which, although an exquisite property of the *apo* form, is also a key determinant of the cAMP-dependent activation of PKA. Table S3 summarizes the values of these five key thermodynamic parameters that reproduce the experimental data of Fig. 4 and are consistent with the available dissociation constants independently measured by stopped flow kinetic measurements (6). Note that, although this two-state mechanism is the simplest model we could propose to fit the experimental data of Fig. 4, we cannot rule out that more complex models (with more than two states) may apply as well. For instance, it is possible the *apo* and C-bound H states may differ, as C binding might quench the dynamics at the R:C interface, including part of the cAMP phosphate binding cassette.

1. Huang H, Melacini G (2006) High-resolution protein hydration NMR experiments: Probing how protein surfaces interact with water and other non-covalent ligands. *Anal Chim Acta* 564(1):1–9.
2. Leon DA, Canaves JM, Taylor SS (2000) Probing the multidomain structure of the type I regulatory subunit of cAMP-dependent protein kinase using mutational analysis: Role and environment of endogenous tryptophans. *Biochemistry* 39(19):5662–5671.
3. Slice LW, Taylor SS (1989) Expression of the catalytic subunit of cAMP-dependent protein kinase in Escherichia coli. *J Biol Chem* 264(35):20940–20946.
4. Iwahara J, Tang C, Marius Clore G (2007) Practical aspects of (1)H transverse paramagnetic relaxation enhancement measurements on macromolecules. *J Magn Reson* 184(2): 185–195.
5. Masterson LR, Mascioni A, Traaseth NJ, Taylor SS, Veglia G (2008) Allosteric cooperativity in protein kinase A. *Proc Natl Acad Sci USA* 105(2):506–511.
6. Anand GS, et al. (2010) Cyclic AMP- and (Rp)-cAMPS-induced conformational changes in a complex of the catalytic and regulatory (RIα) subunits of cyclic AMP-dependent protein kinase. *Mol Cell Proteomics* 9(10):2225–2237.

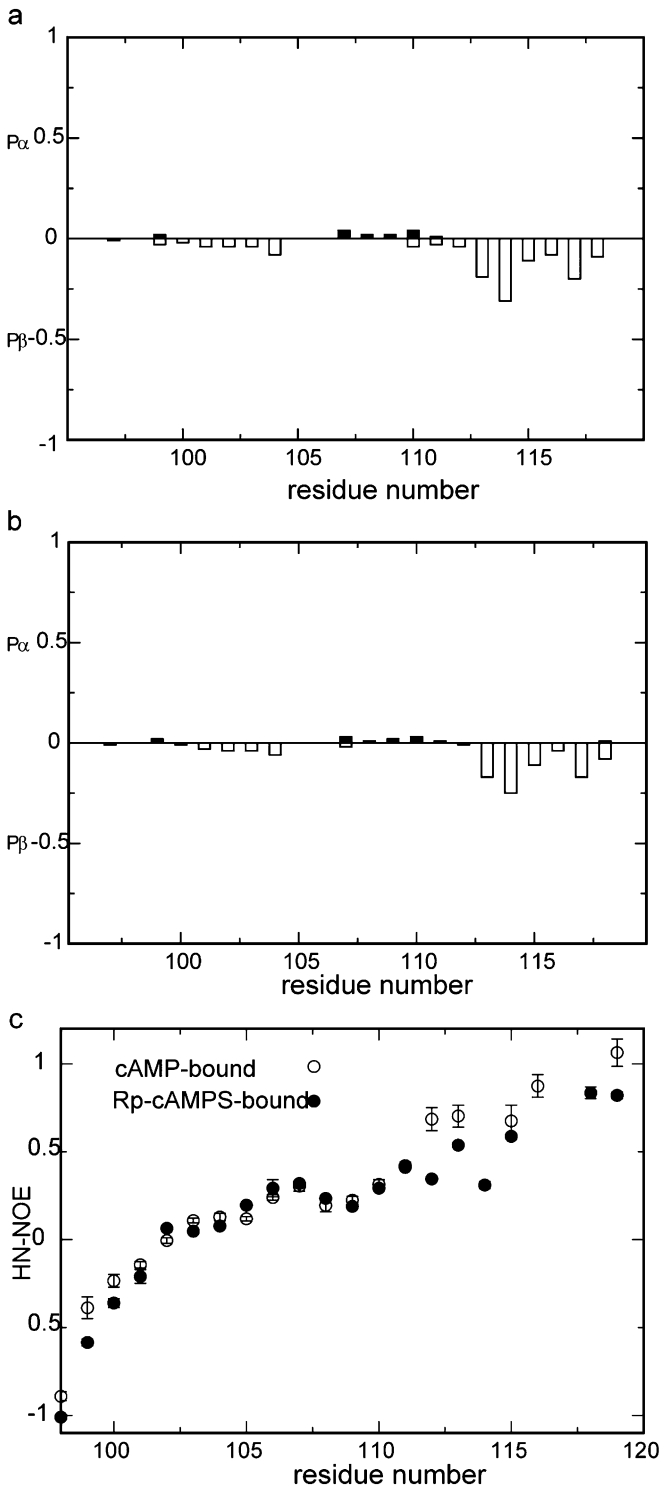

Fig. S1. Lack of well-defined secondary structure in the linker as confirmed by the secondary structure probabilities of the RIα linker (97-120) computed based on the observed chemical shifts using the PECAN software (1) for (*A*) cAMP-bound and (*B*) Rp-cAMPS-bound RIα. The α-helix and β-strand probabilities are reported as positive and negative values, respectively. The RIα (96-244) construct was used because of its solubility at the concentrations required for the acquisition of triple resonance experiments. (*C*) The linker appears quite flexible in the picosecond–nanosecond timescale, as indicated by the HN-NOEs measured for the RIα linker (97-120) residues in cAMP-bound (open circles) and Rp-cAMPS-bound (filled circles) RIα (96-244). This construct was used because of its solubility at the concentrations required for the measurement of reliable HN-NOE values.

1. Eghbalnia HR, Bahrami A, Wang L, Assadi A, Markley JL (2005) Probabilistic identification of spin systems and their assignments including coil-helix inference as output (PISTACHIO). *J Biomol NMR* 32(3):219–233.

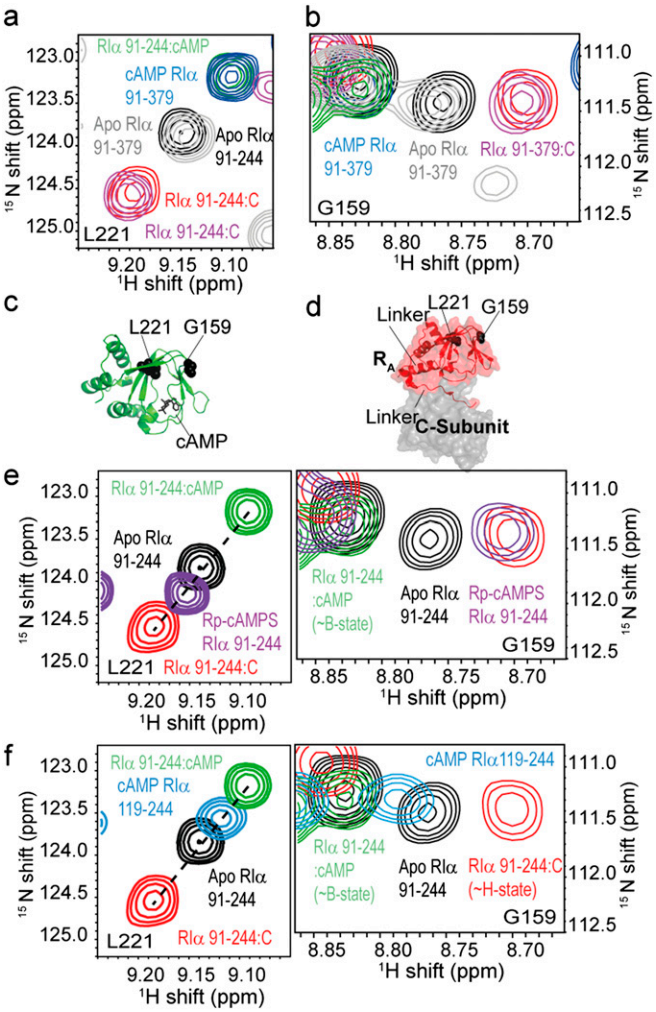

Fig. S2. Position of the H vs. B equilibrium of CBD-A in *apo*, cAMP-, and C-bound RIα (91–244) and RIα (91–379), as sensed by the HSQC peak of L221 (*A*) and G159 (*B*). Whenever R is bound to C, TROSY spectra were acquired. Location of L221, G159 relative to the C-subunit (*C*) and cAMP (*D*) binding interfaces in H and B conformation. Representative H-N correlation peaks for Rp-cAMPS bound RIα (91-244) (purple) (*E*) or cAMP bound RIα (119–244) (cyan) (*F*).

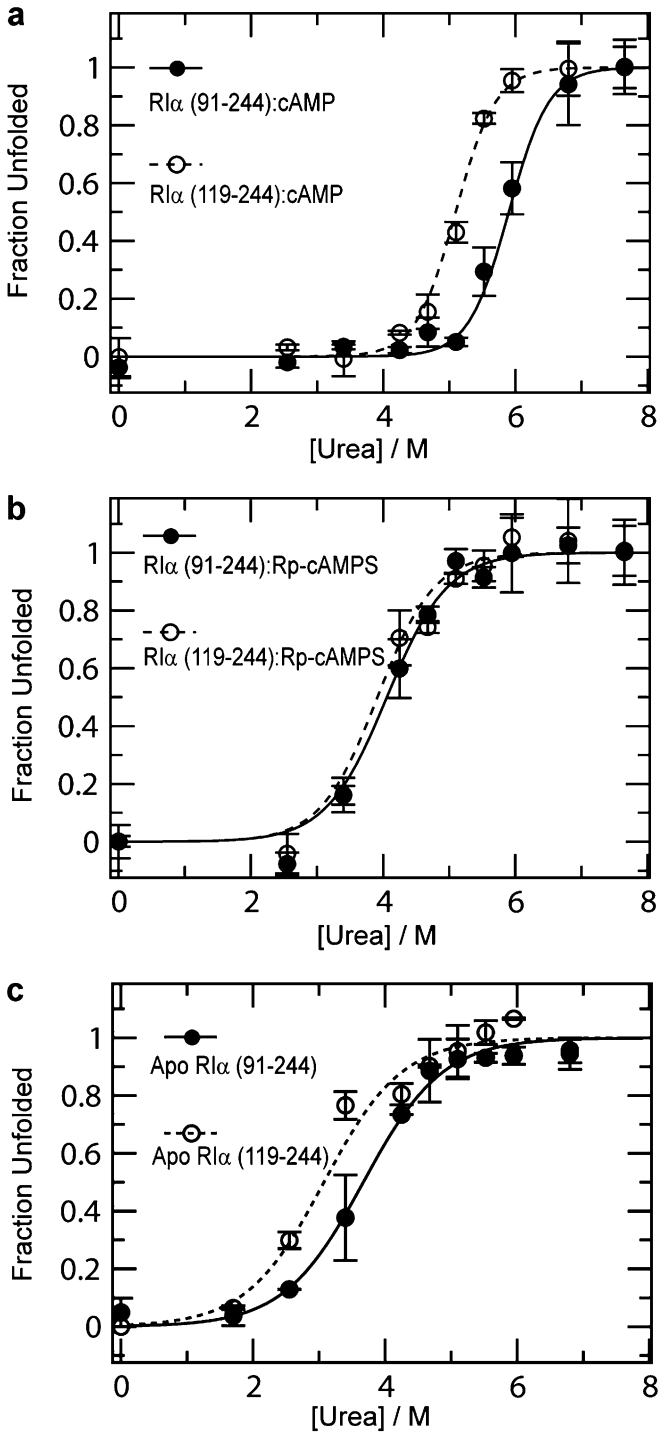

Fig. S3. Effect of the RIα (91-118) linker deletion on the urea-induced unfolding of CBD-A bound to either cAMP (*A*) or the reverse-agonist Rp-cAMPS (*B*) or in the *apo* state (*C*). Symbol legends are embedded in the figure. Fluorescence data report primarily on the unfolding of the globular CBD-A. Boundaries of CBD-A are defined by its noncontiguous α-subdomain with three N-terminal helices starting from residue 119 and a C-terminal helix ending at residue 244 (Fig. 1C), as shown through local spatial pattern alignment methods (1).

1. Kornev AP, Taylor SS, Ten Eyck LF (2008) A generalized allosteric mechanism for cis-regulated cyclic nucleotide binding domains. *PLOS Comput Biol* 4(4):e1000056.

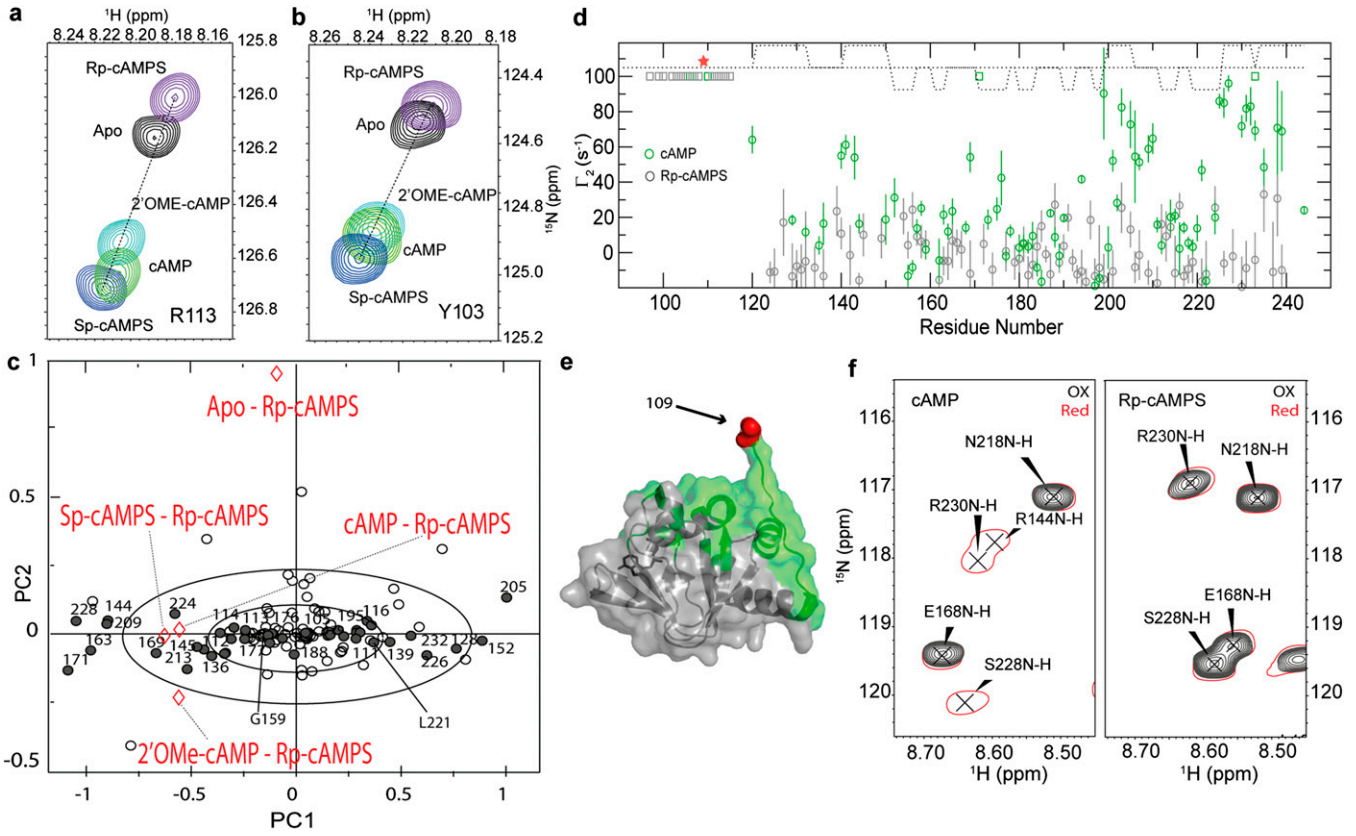

Fig. S4. Chemical shift covariance analysis (CHESCA) and the comparison of PRE profiles observed for cAMP- and Rp-cAMPS-bound RIα (91-244). (*A* and *B*) Representative cross-peaks from the HSQC spectra used for CHESCA: *apo*, cAMP, 2′-OMe-cAMP, Sp-cAMPS, and Rp-cAMPS-bound RIα (91-244). (*C*) SVD of the chemical shift matrix referenced to the Rp-cAMPS-bound state (1) Because the first two PCs alone account for more than 90% of the total variance (Table S2), the PC1 vs. PC2 map of the residue-specific scores (black circles) and of the perturbation-specific loadings (red diamonds) is shown. Ellipsoids at 1 and 2 SDs for the first two PCs are displayed with solid black lines. PC1 reports primarily on allosteric activation as opposed to binding. Unlike PC1, the second PC reports mainly on binding rather than activation. The scores for the residues in the largest AC cluster (Fig. 3*B*) are distributed mostly along PC1 (gray filled circles), confirming that this network is functionally linked to the cAMP-dependent allosteric activation of PKA. (*D*) H^N Γ_2-rates quantified for a sample with a nitroxide at the 109 position (indicated by a red star). Green circles refer to the cAMP-bound state, whereas black circles are for the Rp-cAMPS-bound state. Squares indicate disappearance of peaks in the oxidized state, which is observed in the linker region (97-118). Overall, the PREs observed in the presence of cAMP are markedly higher than those detected with the Rp-cAMPS reverse-agonist, as expected based on the B vs. H preferential interactions of the linker. (*E*) Map of the residues for which the Γ_2-rates in the B state exceed the average + 1 SD [green surface and ribbon representation; Protein Data Bank (PDB) code 1NE6]. The locations of the PRE spin-label (Ala109Cys) are indicated in red. The CBD-A residues experiencing the most significant PREs are those on the side of the CBD-A proximal to the linker in the cAMP-bound state. (*F*) Representative $^1H^{15}N$ HSQC expansions. The spectra recorded with nitroxide in the oxidized (black) and reduced states (red) are shown for both the cAMP- and Rp-cAMPS-bound forms.

1. Selvaratnam R, Chowdhury S, VanSchouwen B, Melacini G (2011) Mapping allostery through the covariance analysis of NMR chemical shifts. *Proc Natl Acad Sci USA* 108(15):6133–6138.

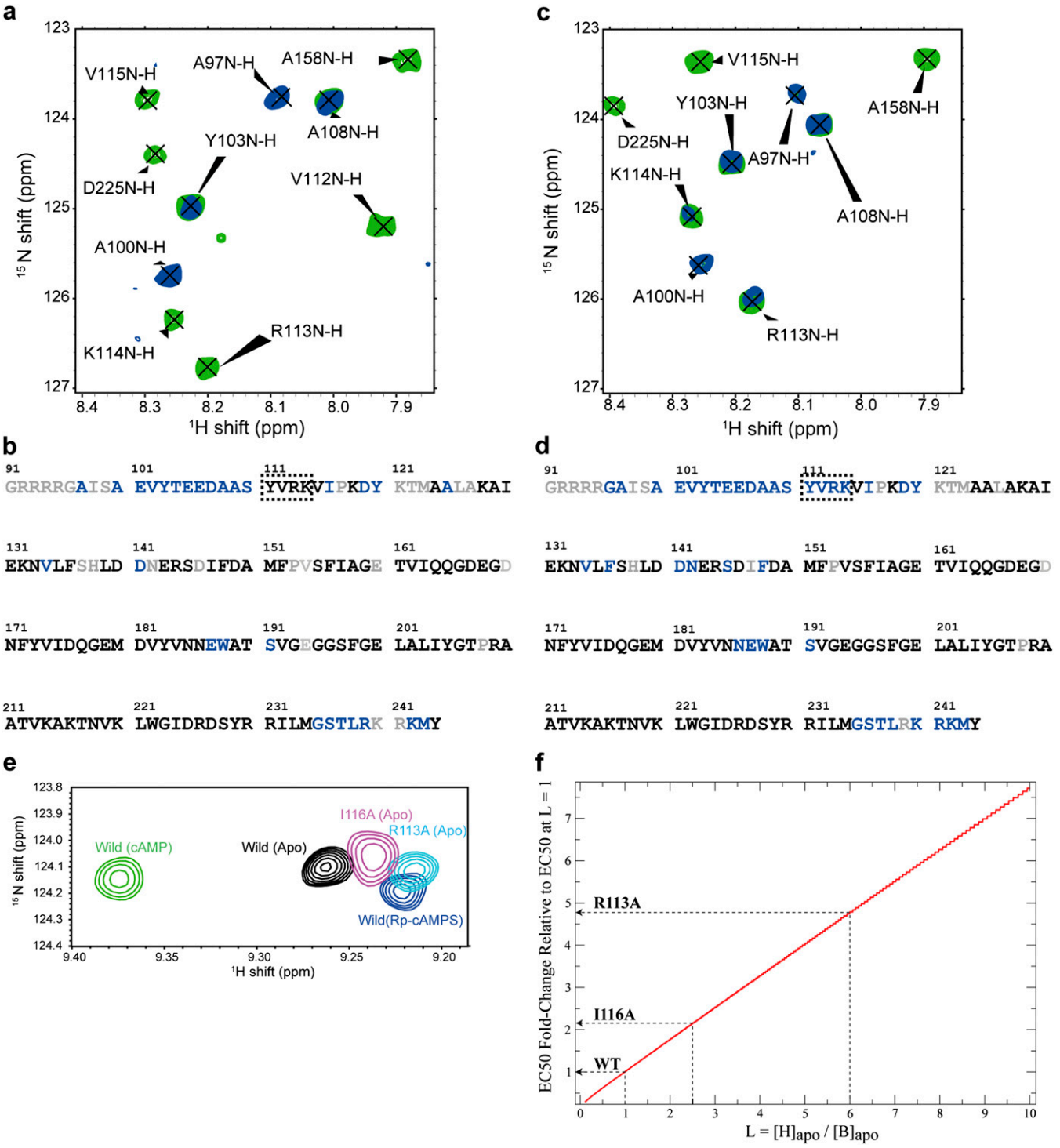

Fig. S5. H/H exchange data for RIα (91-244) bound to either cAMP (*A* and *B*) or Rp-cAMPS (*C* and *D*) The H/H exchange spectra were acquired for both the cAMP- and the Rp-cAMPS-bound forms of R_A, because these ligands stabilize the B and H states of CBD-A, respectively. (*A* and *C*) Representative HSQC (green) and CLEANEX (blue) cross-peaks. (*B* and *D*) RIα (91-244) sequence with residues for which CLEANEX cross-peaks were observed marked in blue. Assigned residues for which CLEANEX cross-peaks were not observed are marked in black. Not-assigned and/or overlapped residues are shown in gray. The comparative cAMP vs. Rp-cAMPS H/H analysis reveals that residues 111-114 (dotted box) are more exposed in the Rp-cAMPS-bound form than in the presence of cAMP, confirming that R113 and the adjacent residues define a key site for the B-selective interaction of the linker with CBD-A. (*E*) Effect of the R113A and I116A mutations on the H vs. B equilibrium of *apo* RIα (91-244) as sensed by the HSQC peak of D140. R113A and I116A mutations shift the H vs. B equilibrium of *apo* RIα (91-244) away from the B state, represented by the cAMP-bound WT RIα (91-244) peak. (*F*) EC_{50} dependence on L, the H vs. B equilibrium constant for *apo* R_A, predicted by the thermodynamic model of Fig. 4*A*. Only the L parameter was varied, with the other four equilibrium constants kept fixed at the values reported in Table S3.

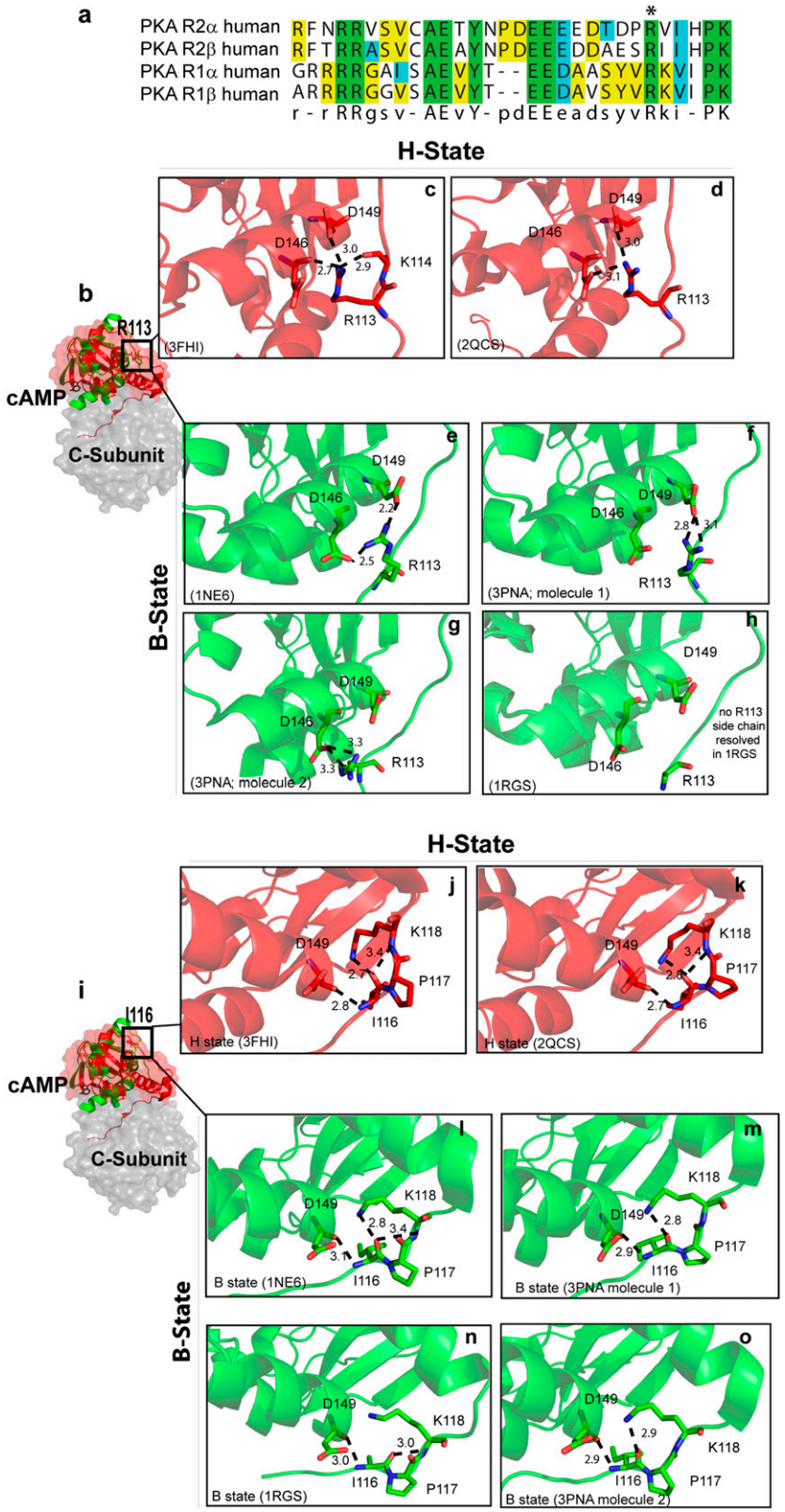

Fig. S6. (*A*) Sequence alignment with CLUSTALW, among the four isoforms of the human R subunit for the region corresponding to the (91-118) linker of RIα. The position of R113 in RIα is marked by an asterisk. (*B*) Location of R113 relative to the cAMP and C-binding interfaces. (*C* and *D*) Hydrogen bonds (dashed lines) formed by the R113 guanidinium in the H-state crystal structures, i.e., C-bound RIα subunit. Note that all residue numbers refer to the R-subunit. (*E–H*) As in *C* and *D* but for the B-state, i.e., cAMP- or Sp-cAMPS-bound RIα subunit. Distances are reported in angstrom. The PDB codes are indicated in parentheses in the figure. The R113 side chain is missing in the 1RGS structure. (*I*) Location of I116 relative to the cAMP and C-binding interfaces. (*J* and *K*) Hydrogen-bonds (dashed lines) formed by I116 in the H-state crystal structures, i.e., C-bound RIα subunit. All residue numbers refer to the R subunit. (*L–O*) As in *J* and *K* but for the B state, i.e., cAMP-, or Sp-cAMPS-bound RIα subunit. Distances are reported in angstrom. The PDB codes are indicated in parentheses in the figure.

Table S1. Summary of urea-induced unfolding thermodynamics data for the (91-244) and (119-244) RIα constructs

RIα constructs	Bound to	C_m, M	$\Delta_{UF}G^{o}_{H2O}$, kcal/mol*	$\Delta_L\Delta_{UF}G^{o}_{H2O}$, kcal/mol†	m, kcal/mol M
(91-244)	cAMP	5.9 ± 0.2	11.4 ± 0.2		−1.9 ± 0.1
(119-244)	cAMP	5.1 ± 0.1	9.9 ± 0.2	1.5 ± 0.3	−1.9 ± 0.1
(91-244)	*–apo*	3.7 ± 0.2	3.6 ± 0.1		−1.0 ± 0.1
(119-244)	*–apo*	3.1 ± 0.2	3.0 ± 0.1	0.6 ± 0.2	−1.0 ± 0.1
(91-244)	Rp-cAMPS	4.0 ± 0.2	5.3 ± 0.2		−1.4 ± 0.1
(119-244)	Rp-cAMPS	4.0 ± 0.1	5.2 ± 0.2	0.1 ± 0.3	−1.3 ± 0.1

*Free energy of unfolding extrapolated to 0 M urea concentration.
†Difference between the $\Delta_{UF}G^{o}_{H2O}$ free energies measured with and without the (91-118) linker. $\Delta_L\Delta_{UF}G^{o}_{H2O}$ quantifies the overall strength of the interactions between the (91-118) linker and the cAMP-binding domain A (CBD-A) of RIα.

Table S2. PC breakdown of total variance

PC	Percentage of total variance, %
PC1	80.1 (80.1)
PC2	11.4 (91.5)
PC3	7.1 (98.6)
PC4	1.4 (100)

Percentages reported in parentheses reflect the cumulative contributions of the PCs in a given row and above.

Table S3. Thermodynamic constants used for the modeling of PKA activation

RIα (91-244)	$K_{a,R(H):C}$, M^{-1}	$K_{a,R(B):C}$, M^{-1}	$K_{a,R(H):cAMP}$, M^{-1}	$K_{a,R(B):cAMP}$, M^{-1}	L
wt	2.5×10^{10}*	3.1×10^{7}†	$\leq 10^{4}$‡	0.5×10^{9}§	1.0¶
I116A	2.5×10^{10}*,‖	3.1×10^{7}†,‖	$\leq 10^{4}$‡,‖	0.5×10^{9}§,‖	2.5§
R113A	2.5×10^{10}*,‖	3.1×10^{7}†,‖	$\leq 10^{4}$‡,‖	0.5×10^{9}§,‖	6.0§

These constants are defined as follows: $K_{a,R(H):C}$ and $K_{a,R(B):C}$ are the association constants between C and RIα (91-244) in the H and B conformations, respectively, whereas $K_{a,R(H):cAMP}$ and $K_{a,R(B):cAMP}$ are the association constants between cAMP and RIα (91-244) in the H and B conformations, respectively. L is the H vs. B equilibrium constant of RIα (91-244) in the absence of cAMP (i.e., *apo* form), as defined in Eq. **S1**.
*$K_{a,R(H):C}$ is approximated as the association constant between C and the reverse agonist Rp-cAMPS-bound RIα (91-244) previously measured by stopped flow kinetic measurements (1).
†$K_{a,R(B):C}$ is approximated as the association constant between C and cAMP-bound RIα (91-244) previously measured by stopped flow kinetic measurements (1).
‡This estimate is based on ref. 2,indicating that cAMP binds the R:C complex with a $K_d > 1$ μM and on the fitting of the activation data for the R113A and I116A mutants.
§Obtained by fitting to the measured activation profile of Fig. 4.
¶L was independently measured using the NMR chemical shifts of Fig. 2.
‖These association constants were assumed to be unaffected by the mutation as the mutated residue is well outside both interfaces with C and cAMP (Fig. S6 *B* and *I*).

1. Anand GS, et al. (2010) Cyclic AMP- and (Rp)-cAMPS-induced conformational changes in a complex of the catalytic and regulatory (RIα) subunits of cyclic AMP-dependent protein kinase. *Mol Cell Proteomics* 9(10):2225–2237.
2. Dao KK, et al. (2006) Epac1 and cAMP-dependent protein kinase holoenzyme have similar cAMP affinity, but their cAMP domains have distinct structural features and cyclic nucleotide recognition. *J Biol Chem* 281(30):21500–21511.